Diffusion at the Surface of Topological Insulators

Pierre Adroguer

Laboratoire de Physique, Ecole Normale Supérieure de Lyon and CNRS UMR5672, France

David Carpentier

Laboratoire de Physique, Ecole Normale Supérieure de Lyon and CNRS UMR5672, France

Jérôme Cayssol

LOMA, University Bordeaux 1, F-33045 Talence, France
Max-Planck-Institut für Physik komplexer Systeme, Nöthnitzer Str. 38, 01187 Dresden, Germany
Department of Physics, University of California, Berkeley, California 94720, USA

Edmond Orignac

Laboratoire de Physique, Ecole Normale Supérieure de Lyon and CNRS UMR5672, France

Abstract. We consider the transport properties of topological insulators surface states in the presence of uncorrelated point-like disorder, both in the classical and quantum regimes. The transport properties of those two-dimensional surface states depend strongly on the amplitude of the hexagonal warping of their Fermi surface. It is shown that a perturbative analysis of the warping fails to describe the transport in experimentally available topological insulators, such as Bi_2Se_3 and Bi_2Te_3. Hence we develop a fully non-perturbative description of these effects. In particular, we find that the dependence of the warping amplitude on the Fermi energy manifests itself in a strong dependence of the diffusion constant on this Fermi energy, leading to several important experimental consequences. Moreover, the combination of a strong warping with an in plane Zeeman effect leads to an attenuation of conductance fluctuations in contrast to the situation of unwarped Dirac surface states.

1. Introduction

Topological insulators (TIs) constitute a new state of matter with an insulating bulk and an odd number of metallic Dirac cones at their surface [1, 2]. It was predicted [3] and confirmed by angle-resolved photoemission spectroscopy (ARPES) [4, 5, 6] that the compounds Bi_2Se_3, Bi_2Te_3 and Sb_2Te_3 possess such a single surface state (SS). Owing to this spin locking property, SSs of TIs are unique metallic systems for the study of fundamental magnetotransport properties and for the realization of future spintronics based devices. Unfortunately such transport experiments have faced a major difficulty so far. Indeed most TIs samples present enough residual bulk conductance to overwhelm the actual surface contribution [7, 8, 9, 10]. The Shubnikov-de Haas oscillations reported in Bi_2Se_3 crystals originate exclusively from the bulk 3D bands indicating a low mobility for the surface Dirac fermions [7, 8, 9]. Nevertheless recent progress has been achieved by using ultrathin films of Bi_2Se_3 [11, 12, 13] or Bi_2Te_3 [14] exfoliated on high-k dielectric insulator in order to improve the surface/bulk conductance ratio and to allow the gating of the surface state. From the gate voltage dependence of the total conductance, it was possible to separate bulk and surface contributions using a classical two-carrier model [11, 12]. Most recently the surface conductance of strained HgTe samples has been reported in truly 3D slabs with thicknesses exceeding 100 nm and in the absence of significant bulk conductance [15]. At low temperatures and for small samples, the quantum correction to transport was recently probed experimentally : the dependence of conductance on weak magnetic fields displays the expected weak antilocalization while the Universal Conductance Fluctuations (UCF) were observed in some of those experiments [14, 11, 15]. Interestingly, the crossover between the symplectic and unitary universality classes upon breaking time-reversal symmetry has been observed in ultrathin samples of Bi_2Te_3 [16].

Theoretically, describing the transport properties of topological insulator surface states amounts to consider the diffusion properties of two dimensional Dirac fermions. Indeed, at the lowest order in $k.p$ theory the SS Fermi surface is circular with a spin winding in the plane. At low energy, this two dimensional conductor shares a lot of similarities with graphene but with the following important differences: the momentum is locked to a real spin as opposed to a A-B sublattice pseudo-spin in graphene, and it has a single Dirac cone as opposed to the four-fold degeneracy of the Dirac cone in graphene. For this simpler Dirac metal, the conductivity and the induced in-plane spin polarization were calculated as functions of the 2D carrier concentration [17]. Far from the Dirac point, surface spin-orbit may generically produce a significant hexagonal warping (HW) of the spin texture. As a result the Fermi surface exhibits a snowflake or a nearly hexagonal Fermi surface depending on the carrier density, and the spin gets tilted out of the plane [18]. Those effects have been confirmed by ARPES and scanning tunneling microscopy (STM) experiments performed on Bi_2Te_3 crystals where HW is particularly strong [19, 20, 21, 22, 23], and also in Bi_2Se_3 [24, 25]. Characterizing quantitatively the HW and therefore the amount of out-of plane spin polarization is a

crucial issue in view of potential spintronics applications, and has been the subject of ab-initio studies [26] and ARPES experiments [22]. This hexagonal warping is specific to the Dirac metal at the surface of topological insulators, and different from the trigonal warping encountered at high energies in graphene. Its amplitude is stronger in the metallic regime of high Fermi energy which is of interest in the present paper : a full description of transport properties in this regime necessitates to include its presence in the model. It has been shown [27, 28] that hexagonal warping enhances perturbatively the classical Drude conductivity with respect to the unwarped model [17]. However, as we will show in this article a description of the effects of this hexagonal warping requires to go beyond the previous perturbative descriptions. In this paper, we develop a description of the diffusion of these surface states which is non-perturbative in the warping amplitude.

We investigate theoretically the classical 2D charge diffusion within an hexagonally warped surface states using both a standard diagrammatic formalism and a Boltzmann equation approach. In this classical regime, we find that the hexagonal warping on one hand strongly reduces the density of states and on the other hand increases the diffusion coefficient for the Dirac surface states. The combination of both effects is found to correspond to an increase of the classical conductivity as a function of the warping amplitude. Interestingly, as the warping amplitude increases with Fermi energy, that dependence on the warping amplitude manifests itself in the behavior of the conductivity as a function of the Fermi energy. In the second part of this article, we focus on the quantum correction to the conductivity, relevant in a phase coherent conductor. These quantum corrections are known to depend on the symmetry class of the associated Anderson localization problem. Similarly to graphene with only intra-valley disorder, the single Dirac cone model is known to correspond to the symplectic / AII class. Within this symplectic class the Dirac model differs from graphene with long-range disorder or electrons with spin-orbit randomness by the presence of a topological term in the associated field theory [29, 30]. This topological term explains the absence of Anderson localization for these topological insulators surface states [31, 32, 33], however it plays no role in the diffusive metallic regime. In this regime, the universal properties of both weak localization and conductance fluctuations are just the same as for any model on the two dimensional symplectic / AII class. We will recall these results, and show that the dependence of the diffusion coefficient on warping manifests itself in a dependence of the weak localization correction and conductance fluctuations away from their universal values. In particular, this diffusion constant parameterizes the universal cross-over from the symplectic / AII class to the unitary / A class when a magnetic field is applied perpendicular to the surface states. The shape of the associated cross-over functions now depends strongly on the warping amplitude, and thus the Fermi energy. Finally, we identify a property unique to the topological insulator surface states : a reduction of the conductance fluctuations by the application of a in-plane magnetic field.

The paper is organized as follows. We present the model in section 2. The classical Drude conductivity in presence of HW is derived using a Boltzmann approach (section

3) and a diagrammatic method (section 4). In section 5, the quantum corrections to the average conductivity and the Universal Conductance Fluctuations are respectively derived. The results and conclusions relevants for experiments are summarized in the conclusive section 6.

2. Model

2.1. Hamiltonian and Warping Potential

We consider the Hamiltonian describing a single species of surface states of a strong topological insulator

$$H = \hbar v_F \ \vec{\sigma} \cdot \vec{k} + \frac{\lambda}{2}\sigma_z(k_+^3 + k_-^3) + V(\vec{r}), \tag{1}$$

where $\vec{\sigma} = (\sigma_x, \sigma_y)$ is the two-dimensional vector of Pauli matrices describing the physical in-plane spin of the electron, and $\vec{k} = (k_x, k_y)$ is its in-plane momentum operator which satisfy the usual commutation relation with the position operator $[r_\alpha, k_\beta] = i\delta_{\alpha\beta}$ $(\alpha, \beta = x, y, z)$. Note that in Eq.(1), we used for sake of simplicity the dispersion relation $\vec{\sigma}\cdot\vec{k}$ for the Dirac part instead of the usual $\vec{\sigma}\times\vec{k}$ hamiltonian : switching from one to the other amounts to perform an in plane $\pi/2$ rotation around z in the spin space and has no consequence on the following discussion as it does not affect the hexagonal warping potential. Concerning the description of the disorder potential $V(\vec{r})$, we will follow the standard description by considering a Gaussian random potential $V(\vec{r})$, characterized by a zero average value $\langle V(\vec{r})\rangle = 0$ and variance $\langle V(\vec{r})V(\vec{r'})\rangle = \gamma\delta(\vec{r} - \vec{r'})$, where $\langle \ldots \rangle$ represents the average over different disorder realizations.

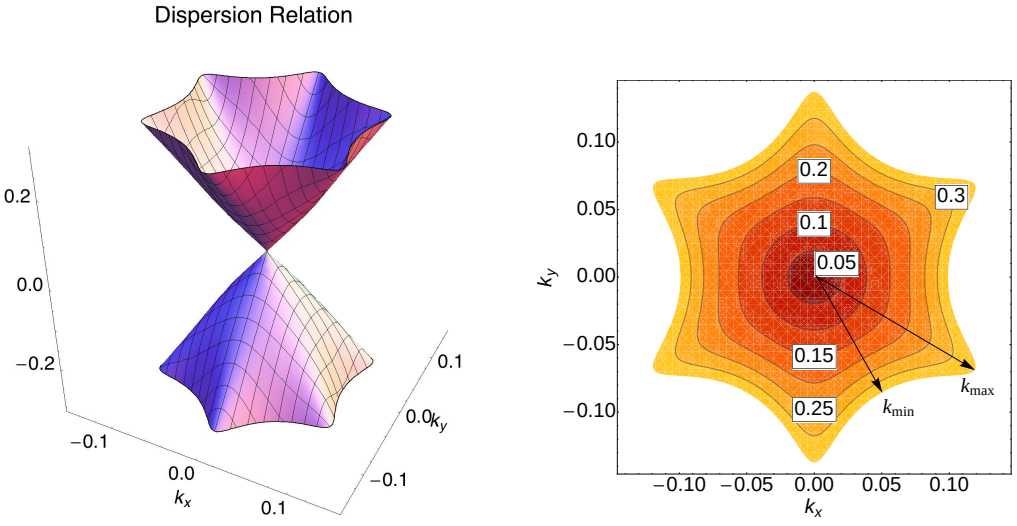

Figure 1. Fermi surface in presence of hexagonal warping for various Fermi energies with parameters relevant for Bi_2Te_3 : $\lambda = 250$ eV.$\mathring{A}^3$ and $v_F = 2.55$ eV.$\mathring{A}$ and Fermi energies from $E_F = 0.05$ eV to 0.3 eV, corresponding to a warping parameter b ranging from 0 to $b \simeq 0.7$.

The hexagonal warping term $H_{\rm W} = \frac{\lambda}{2}\sigma_z(k_+^3 + k_-^3)$, with $k_\pm = k_x \pm ik_y$, breaks the full $U(1)$ rotation symmetry of the Dirac cone down to a trigonal discrete C_3 symmetry [18, 34]. Time reversal symmetry leads to an additional hexagonal C_6 symmetry of the Fermi surface, hence the name hexagonal warping (Fig.1). The dispersion relation in the absence of disorder with $\vec{k} = (k_x, k_y) = k(\cos\theta, \sin\theta)$:

$$\epsilon^2(\vec{k}) = \hbar^2 v_F^2 k^2 + \lambda^2 k^6 \cos^2(3\theta), \tag{2}$$

is obtained by squaring the Hamiltonian Eq.(1) with $V(\vec{r}) = 0$, and leads to the snowflake shape of equal energy surfaces at high energies : see Fig.1. Defining $E_F = \hbar v_F k_F$ and $k = k_F \tilde{k}(\theta)$, the shape of the Fermi surface at energy E_F is defined by the equation

$$1 = \tilde{k}^2(\theta) + 4b^2\tilde{k}^6(\theta)\cos^2(3\theta). \tag{3}$$

Hence the warping of this Fermi surface is naturally characterized by the dimensionless parameter

$$b = \frac{\lambda E_F^2}{2\hbar^3 v_F^3}, \tag{4}$$

which will play a crucial role in the remaining of this paper. This parameter is related to geometrical warping deformation factor w introduced in ref. [22], and defined from the maximum and minimum momenta k_{max}, k_{min} of a constant energy contour (see Fig.1) as

$$\tilde{w} = \frac{w}{w_{max}} = \frac{k_{max} - k_{min}}{k_{max} + k_{min}} \quad \text{with} \quad w_{max} = \frac{2+\sqrt{3}}{2-\sqrt{3}} \simeq 13.9 \tag{5}$$

With the notations of Eq. (3), we have $k_{min}/k_{max} = \tilde{k}(\theta = 0)$, leading to the expression

$$b(w) = \frac{\sqrt{\tilde{w}}(1+\tilde{w})^2}{(1-\tilde{w})^3} = \sqrt{w w_{max}}\frac{(w_{max}+w)^2}{(w_{max}-w)^3}. \tag{6}$$

Two values appear remarkable : $w = 0, b = 0$ correspond to a circular Fermi Surface ; $w = 1, b = 2/(3\sqrt{3}) \simeq 0.38$ to a hexagonal Fermi surface; while $w > 1$ indicates a snowflake shape.

Using the experimental values for the Bi_2Se_3 compound $\lambda = 128$ eV.$\mathring{A}^3$, $v_F = 3.55$ eV.$\mathring{A}$ from [24] we obtain relatively small values of warping $0.04 < b < 0.09$ for energies $0.05eV < E < 0.15eV$, and similarly $0.0 < b < 0.04$ with the values $\lambda = 95$ eV.$\mathring{A}^3$, $v_F = 3.0$ eV.$\mathring{A}$ and 0.00eV $< E <$ 0.15eV from [25]. On the other hand, the experimental values for the Bi_2Te_3 compound $\lambda = 250$ eV.$\mathring{A}^3$ and $v_F = 2.55$ eV.$\mathring{A}$ [5, 19] lead to a warping factor ranging from $b = 0.13$ for $E = 0.13$ eV to $b = 0.66$ for $E = 0.295$ eV. As we will show below, these large values of warping amplitude are indeed beyond the reach of a perturbative approach, and require a non-perturbative description of diffusion in the presence of warping.

3. Classical Drude conductivity: Boltzmann equation

The momentum relaxation rate in presence of warping can be obtained from a simple application of Fermi's Golden Rule:

$$\frac{1}{\tau_e} = \int \frac{d\vec{k'}}{(2\pi)^2} 2\pi |\langle \vec{k'}|\vec{k}\rangle|^2 \gamma \delta(\epsilon(\vec{k'}) - E_F), \tag{7}$$

where $\langle \vec{k'}|\vec{k}\rangle$ is the overlap between the eigenstates labelled by $\vec{k}$ and $\vec{k'}$ at the Fermi surface. The disorder strength is characterized by $\gamma = n_i V^2$, and the dispersion $\epsilon(\vec{k})$ is given by Eq. (2).

At equilibrium, the occupation numbers are given by the Fermi distribution $n_F(\epsilon(\vec{k}))$. In presence of a finite external electric field $\vec{E}$, the occupation number function $f(\vec{k})$ has to be determined by solving the Boltzmann equation:

$$-e\vec{E}.\frac{\partial f(\vec{k})}{\partial \vec{k}} = \int \frac{d\vec{k'}}{(2\pi)^2} 2\pi n_i |\langle \vec{k'}|V|\vec{k}\rangle|^2 \delta(\epsilon(\vec{k'}) - \epsilon(\vec{k})) \left[f(\vec{k'}) - f(\vec{k}) \right]. \tag{8}$$

This equation is nontrivial to solve due to both the warped shape of the Fermi surface and the anisotropy of the scattering. Indeed, even if the scalar disorder is isotropic and spin diagonal, the spin-locking property makes the scattering anisotropic (even for a circular unwarped Fermi surface). This anisotropy is further increased by the hexagonal warping of the Fermi surface. This is apparent when considering the scattering amplitude which appears in Eq.(8) : $f(\theta, \theta' - \theta) = |\langle \vec{k}|V|\vec{k'}\rangle|$ between eigenstates of the disorder-free Hamiltonian $H_0 + H_{\rm W}$ in Eq.(1), as a function of the polar angle θ on the incident state $|\vec{k}\rangle$ and polar angle θ' of the outgoing state $|\vec{k'}\rangle$. Due to the presence of hexagonal warping, this scattering amplitude is highly spin-dependent and anisotropic along the Fermi surface, especially at large Fermi energy where the warping factor b is large. Moreover this amplitude $f(\theta, \theta' - \theta)$ becomes dependent on the incident state direction θ, and not only on the relative angle, $(\theta' - \theta)$ as opposed to the case of Dirac fermions without warping. These properties are represented in Fig. 2.

To solve the equation (8), we use the linearized ansatz:

$$f(\vec{k}) = n_F\left(\epsilon(\vec{k})\right) + \frac{\partial n_F}{\partial \epsilon} \bar{f}(\theta), \tag{9}$$

where the angular function $\bar{f}(\theta)$ is linear in electric field. We find:

$$-e\vec{E}.\frac{\partial \epsilon}{\partial \vec{k}} = 2\pi\gamma \int \frac{d\theta'}{(2\pi)^2} |\langle \vec{k'}|\vec{k}\rangle|^2 k_{F\theta'} \left(\frac{\partial \epsilon}{\partial k}\right)^{-1}_{\theta'} \left[\bar{f}(\theta') - \bar{f}(\theta) \right], \tag{10}$$

where the Fermi wavevector $k_{F\theta'}$ and the derivative $(\partial\epsilon/\partial k)_{\theta'}$ are both evaluated at the point of the Fermi surface labelled by the angle θ'. The solution of this integral equation at fourth order in b is:

$$\begin{aligned} \bar{f}(\theta) = ev_F\tau_e E_x \Big[& 2\cos\theta + b^2 \left(18\cos\theta + 5\cos(5\theta) - \cos(7\theta)\right) \\ & - \frac{b^4}{4}\left(522\cos\theta + 20\cos(5\theta) + 44\cos(7\theta) + 49\cos(11\theta) - 11\cos(13\theta)\right) \Big]. \end{aligned} \tag{11}$$

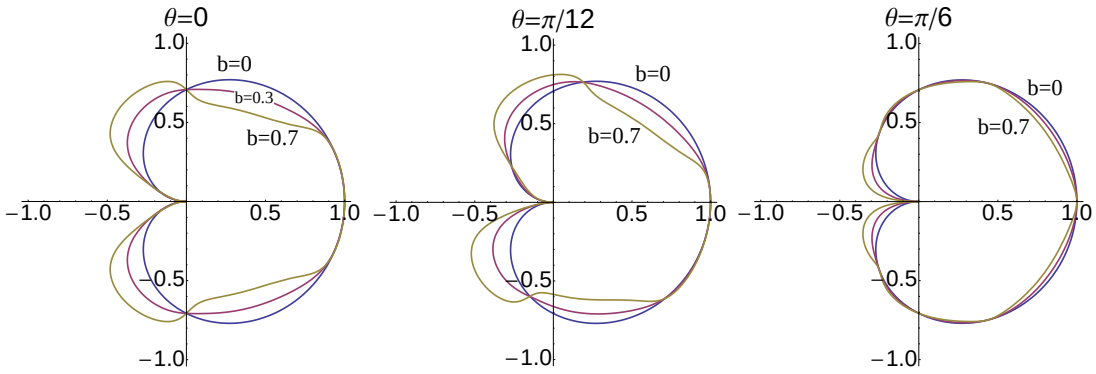

Figure 2. Scattering amplitude $|\langle\vec{k}|V|\vec{k'}\rangle|^2$ plotted as a function of the relative angle $\theta' - \theta$ between the incident state $\vec{k}$ of polar angle θ and the scattered state $\vec{k'}$ of polar angle θ'. Three different incident directions are plotted to demonstrate the dependence on the polar angle of the incident state : $\theta = 0, \pi/12, \pi/6$, while the results are invariant by $\pi/3$ rotation of the incident state. The results are shown for increasing energies warping factor $b = 0 - 0.7$ corresponding to increasing Fermi energies in a given material.

The current is then calculated as:

$$j_x = \int \frac{d\vec{k}}{(2\pi)^2} e \frac{\partial \epsilon}{\partial k_x} \bar{f}(\theta) \delta(\epsilon(\vec{k}) - E_F) = \sigma E_x, \tag{12}$$

leading to the conductivity:

$$\sigma = \sigma^{(0)} \left(1 + 8b^2 - 58b^4 + o(b^4)\right). \tag{13}$$

The conductivity and density of states (at Fermi level) in the absence of warping ($b = 0$) are given respectively by $\sigma^{(0)} = e^2 \rho^{(0)} v_F^2 \tau_e^{(0)}$ and $\rho^{(0)} = \frac{E_F}{2\pi\hbar^2 v_F^2}$. Similarly, one can also derive the perturbative (and non-perturbative) expression for the density of state ρ : this is done in Appendix A and the result is represented on Fig. 3. However, to go beyond the above perturbative expansion for the conductivity, a diagrammatic approach turns out to be more convenient. Hence we proceed below by developing such an approach, comparing its results with the perturbative expansion of Eq. (13).

4. Classical Drude conductivity : diagrammatic approach

In this part, we investigate within the standard diagrammatic framework the diffusive transport of Dirac surface state with an arbitrary large warping deformation (see Eq. (1)). We start by calculating the single particle Green function averaged over disorder whose imaginary part yields the density of states. Then we evaluate the classical Drude conductivity from the bubble diagram containing two dressed current operators linked by two disorder averaged Green functions. We discuss the dependence of the classical conductance as a function of the 2D carrier density and the HW coupling strength.

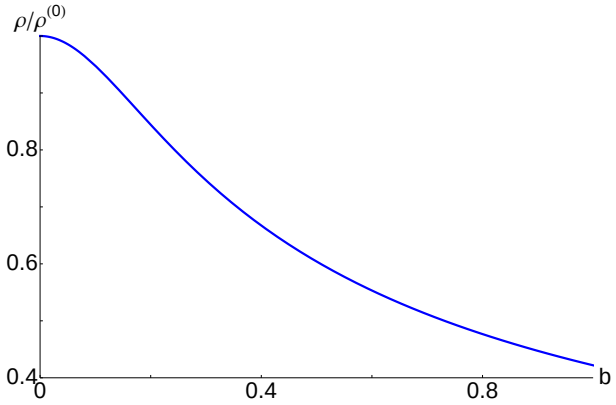

Figure 3. Renormalization of the density of states $\rho(E_F)$ by the warping of the surface states, non perturbatively in the warping amplitude b. The resulting correction is represented $\rho(E_F)/\rho^{(0)}$ where $\rho^{(0)} = \rho(\lambda = 0)$ is the density for Dirac Fermions without warping.

4.1. Averaged Green's function and elastic scattering time.

The averaged Green's function is obtained by calculating the self-energy correction and averaging over disorder [35]. The corresponding disorder averaged propagator reads:

$$\langle G^{R/A}(\vec{k})\rangle = \frac{(E \pm i\hbar/2\tau_e)\mathbb{1} + \hbar v_F \vec{k}\ .\ \vec{\sigma} + \lambda k^3 \cos(3\theta)\sigma^z}{(E \pm i\hbar/2\tau_e)^2 - \hbar^2 v_F^2 k^2 - \lambda^2 k^6 \cos^2(3\theta)} \tag{14}$$

where the elastic scattering time for the warped (resp. unwarped) conical Dirac fermion τ_e (resp. $\tau_e^{(0)}$) is defined by :

$$\rho\tau_e = \rho^{(0)}\tau_e^{(0)} = \frac{\hbar}{\pi\gamma}. \tag{15}$$

We assume that the phase coherence time $\tau_\phi \gg \tau_e$ in order to be in the regime of coherent transport. By using the parameterization $\tilde{k}(\theta)$ of the Fermi surface shape introduced in Eq. (3), we obtain the non perturbative expression for the the density of states :

$$\frac{\rho}{\rho^{(0)}} = \alpha(b) = \int_0^{2\pi} \frac{d\theta}{2\pi} \frac{1}{1 + 12\ b^2\tilde{k}^4(\theta)\cos^2(3\theta)} = \frac{\tau_e^{(0)}}{\tau_e} \tag{16}$$

We find an increase of the scattering time τ_e by the warping. Hence in the presence of hexagonal warping, the surface states of topological insulators are relaxing carrier momentum less effectively than without warping. This is a manifestation of the increased anisotropy of the scattering amplitude by the hexagonal warping correction, illustrated in Fig.2. Indeed in the presence of hexagonal warping, the neighboring states of an incident Dirac fermions have smaller overlaps than states that are $\pm 2\pi/3$ apart, which effectively induces a very anisotropic scattering. Nevertheless from this result, one can not yet conclude that the Drude conductance is enhanced as the density of states at the Fermi energy is also renormalized by the warping. Indeed the Drude conductance is determined by the diffusion constant D and the transport relaxation time rather than the elastic scattering time τ_e governing momentum relaxation. To access this classical conductivity, we follow the standard diagrammatic procedure in the following section.

4.2. Diagrams for the classical conductivity

For a given impurity configuration, the conductivity is given by the Kubo formula :

$$\sigma = \sigma_{xx} = \frac{\hbar}{2\pi L^2} \Re \mathrm{Tr} \left[j_x G^R j_x G^A \right], \tag{17}$$

where we have neglected subdominant contributions involving products $G^R G^R$ and $G^A G^A$ [36]. In this expression and below, Tr denotes a trace over the electron's Hilbert space (momentum and spin quantum numbers). The current operator j_α is obtained from the Hamiltonian Eq. (1) by inserting the vector potential *via* the minimal coupling substitution $\vec{k} \to \vec{k} - (e/\hbar)\vec{A}$ and using the definition $j_\alpha = \frac{\delta H}{\delta A_\alpha}$:

$$j_x = (-e) \left(v_F \ \sigma_x + \frac{3\lambda}{\hbar} \sigma_z (k_x^2 - k_y^2) \right). \tag{18}$$

Note that this current contains the usual $-ev_F\sigma_x$ term for linearly dispersing Dirac system, and an additional term quadratic in momentum originating from the HW.

After averaging over all impurity configurations, the classical mean conductivity is obtained from the bubble diagram of Fig. 4 where the propagating lines represent the retarded and advanced disorder averaged Green functions Eq. (14). This classical conductivity is the sum of two terms : σ_A and σ_B. The contribution of diagram A in

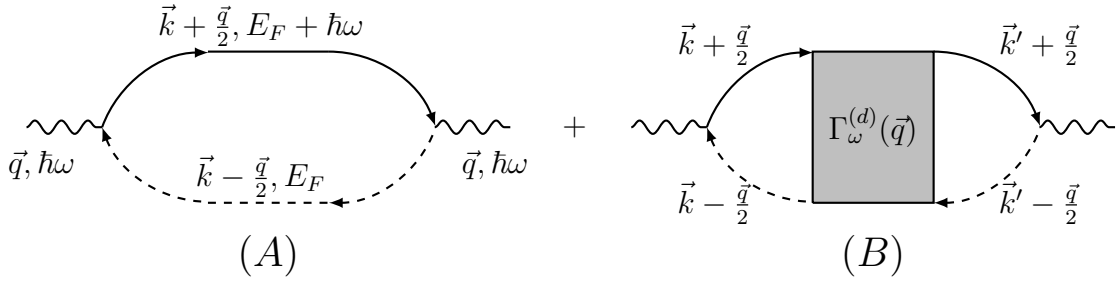

Figure 4. Diagrammatic representation of the two contributions σ_A and σ_B to the classical conductance

Fig. 4 is defined at $\vec{q} = 0$ and $\omega = 0$ by

$$\sigma_A = \frac{\hbar}{2\pi} \int \frac{d\vec{k}}{(2\pi)^2} \ \mathrm{tr} \left[j_x(\vec{k}) \langle G^R(\vec{k}, E_F) \rangle j_x(\vec{k}) \langle G^A(\vec{k}, E_F) \rangle \right], \tag{19}$$

where tr denotes a trace only over the spin quantum numbers. Performing explicitly the trace and the integration over the momentum $k = |\vec{k}|$, we obtain the following expression:

$$\sigma_A = \frac{\hbar e^2 v_F^2}{2\pi\gamma} \frac{\alpha(b) + 5\beta(b) + \delta(b)}{\alpha(b)}, \tag{20}$$

which is non perturbative in b. The function $\alpha(b)$ has been defined in Eq.(16) and we have introduced :

$$\alpha(b) = \int_0^{2\pi} \frac{d\theta}{2\pi} \frac{1}{1 + 12 \ b^2 \tilde{k}^4(\theta) \cos^2(3\theta)} \tag{21}$$

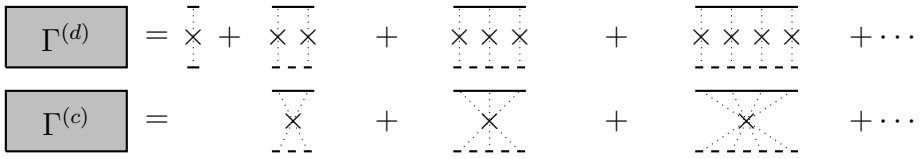

Figure 5. Schematic representation of the Diffuson and Cooperon structure factors. The dotted lines correspond to disorder correlators, while the plain and dashed lines represent retarded and advanced Green's functions.

$$\beta(b) = \int_0^{2\pi} \frac{d\theta}{2\pi} \frac{4b^2 \cos^2(3\theta)\tilde{k}^6(\theta)}{1 + 12b^2 \cos^2(3\theta)\tilde{k}^4(\theta)}, \tag{22}$$

$$\delta(b) = \int_0^{2\pi} \frac{d\theta}{2\pi} \frac{36b^2(\tilde{k}^4(\theta) - \tilde{k}^6(\theta))}{1 + 12b^2 \cos^2(3\theta)\tilde{k}^4(\theta)}, \tag{23}$$

where $k = k_F\tilde{k}(\theta)$ with $\tilde{k}(\theta)$ introduced in Eq. (3).

The contribution of the diagram B in Fig. 4 accounts for the contribution of the so-called Diffuson [36]. Retaining only the dominant contribution of the integral, we can write it explicitly as

$$\sigma_B(\vec{q},\omega) = \frac{\hbar}{2\pi}\mathrm{tr}\left[J_x\Gamma^{(d)}(\vec{q},\omega)J_x\right], \tag{24}$$

where the vertex operator J is defined by

$$J_x = \int \frac{d\vec{k}}{(2\pi)^2}\langle G^A(\vec{k},E)\rangle\ j_x(\vec{k})\ \langle G^R(\vec{k},E)\rangle = J\ \sigma_x. \tag{25}$$

A contraction over the spin indices is assumed, resulting in the proportionality to σ_x.

The Diffuson structure factor $\Gamma^{(d)}$ in Eq.(24) is defined diagrammatically in Fig. 5, and satisfies the usual recursive Dyson equation, solved by the expression $\Gamma^{(d)}(\vec{q},\omega) = \gamma\left[\mathbb{1}\otimes\mathbb{1} - \gamma P^{(d)}(\vec{q},\omega)\right]$ where $P^{(d)}$ is the polarizability

$$P^{(d)}(\vec{q},\omega) = \int \frac{d\vec{k}}{(2\pi)^2}\langle G^R(\vec{k},E)\rangle \otimes \langle G^A(\vec{k}-\vec{q},E-\omega)\rangle, \tag{26}$$

where $\otimes$ denotes a tensor product of the spin Hilbert spaces. The resulting structure factor $\Gamma^{(d)}$ is naturally decomposed into 4 spin modes. However, as opposed to the case of non-relativistic electrons [36], for finite but small q, the non-diagonal character of the Dirac Green's functions leads to unusual terms in this structure factor such as $(\vec{q}.\vec{\sigma})\otimes(\vec{q}.\vec{\sigma}), (\vec{q}.\vec{\sigma})\otimes\mathbb{1}$. We recover the standard singlet and triplets states only in the diffusive $q \to 0$ limit. In this limit, the only gapless mode is the singlet state, characteristic of the symplectic / AII class. While this mode and the associated Cooperon singlet determines the quantum corrections to diffusion, it does not contribute to the classical conductivity of Eq. (24). The only classical contribution comes from one of the massive triplet states. In full generality, the $q \to 0$ limit of the structure factor $\Gamma^{(d)}$ can be parameterized according to

$$\Gamma^{(d)} = a_1\mathbb{1}\otimes\mathbb{1} + a_2(\sigma^x\otimes\sigma^x + \sigma^y\otimes\sigma^y) + a_3\sigma^z\otimes\sigma^z. \tag{27}$$

Using the parameterization of Eq. (25) and performing the resulting trace we obtain :

$$\sigma_B = j^2(a_1 - a_3) = \frac{\hbar e^2 v_F^2}{2\pi\gamma} \frac{(\alpha(b) + 2\beta(b))^2}{\alpha(b)(\alpha(b) + \beta(b))} \tag{28}$$

Adding the two contributions of Eq. (20) and (28) leads to the full expression for the classical conductivity :

$$\sigma_{cl} = \sigma_A + \sigma_B = e^2 \rho D. \tag{29}$$

The evolution of this classical conductivity as a function of the warping amplitude is represented in Fig. 6. Moreover, this expression of the conductivity allows us to define

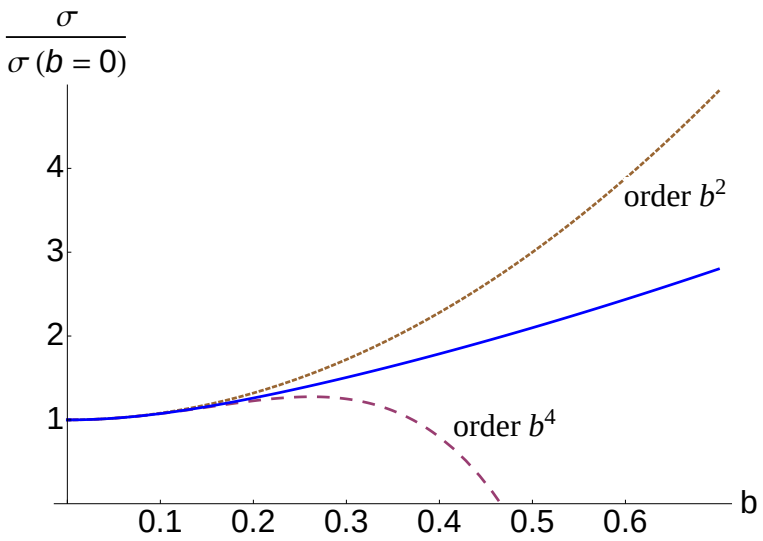

Figure 6. Longitudinal conductivity as a function of the parameter b. Solid line is the exact calculation, dotted line is the 4th order expansion in b calculated through the Boltzmann equation, dashed line is the 2nd order.

the diffusion constant D from the Einstein relation, whose final expression reads

$$D = \frac{v_F^2 \tau_e}{2} \left(\frac{\alpha(b) + 5\beta(b) + \delta(b)}{\alpha(b)} + \frac{(\alpha(b) + 2\beta(b))^2}{\alpha(b)(\alpha(b) + \beta(b))} \right) \tag{30}$$

which is non perturbative in the warping parameter b. In the limit $b \to 0$ of absence of warping, we recover the known result for Dirac fermions in the presence of a scalar disorder with a diffusion constant $D = v_F^2 \tau_e = v_F^2 \tau_{tr}/2$ and a transport time $\tau_{tr} = 2\tau_e$ accounting for the inherent anisotropic scattering of Dirac fermions on scalar disorder. The renormalized diffusion constant is found to increase as a function of b (Fig. 7). This dramatic increase of D within the range of experimentally relevant warping parameter b signals an effective strong increase of the anisotropy of scattering when hexagonal warping is present. Note that in the present case, this diffusion coefficient accounts for both the renormalization of the averaged Fermi velocity and the scattering amplitude corresponding to a renormalized transport time. Moreover, the comparison of the expression of Eq. (30) with its perturbative expansion to order b^4 demonstrates that the experimental values of warping b are beyond the reach of this perturbative

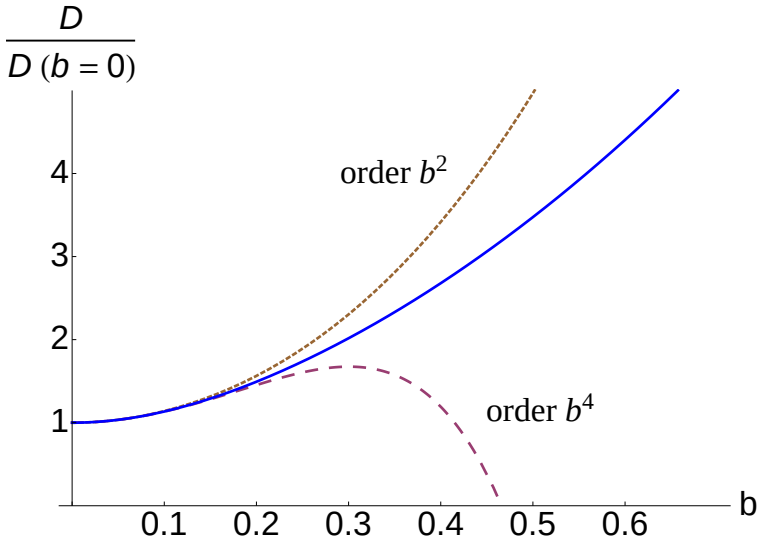

Figure 7. Evolution of the diffusion constant as a function of warping intensity b. The solid line corresponds to the expression non perturbative in the warping amplitude b, while the dotted and dashed curves correspond to perturbative results to order b^2 and b^4.

expansion (and the similar perturbative studies of [27, 28]) : to describe accurately the experimental situation at high doping, the full exact expression Eq. (30) is required.

5. Quantum corrections to the conductivity

In this section, we focus on the regime of quantum transport corresponding to a phase coherent diffusion of the surface states which can be reached for small sample size and at low temperatures. This regime corresponds to the situation where the Fermi momentum k_F satisfies the condition $k_F l_e \gg 1$, which naturally corresponds to the situation where the warping of the Fermi surface is strong. We focus on the first two cumulants of the distribution of conductivity and compute diagrammatically the corresponding quantum corrections non perturbatively in the warping amplitude b, extending the results of Refs. [27, 28].

5.1. Universality classes

The study of non-interacting metals perturbed by disorder corresponds to the well-studied problem of Anderson localization of electronic waves. In this framework, the transport properties depend on both dimension and universality classes determined by the symmetries preserved by disorder. These universality classes encodes both the universal properties of the Anderson transition, but also the universal properties of the weak disorder metallic regime of interest experimentally in the present case. The model considered in this paper $H = \hbar v_F \vec{\sigma} \cdot \vec{k} + V(\vec{r})$ is described at large distances by the standard AII / symplectic class : time-reversal symmetry T is preserved, but due to

the momentum-spin locking it squares to $T^2 = -\mathrm{Id}$ [37, 38]. This is also the Anderson universality class describing non-relativistic electrons in the presence of random spin orbit disorder. However while both models possess the same universal weak localization properties, they differ in their strong disorder behavior : the topological nature of the single Dirac species in the present model manifest itself in the appearance of a topological term in the field-theoretic description of the $d = 2$ AII class [29, 30]. The presence of this topological $\mathbb{Z}_2$ term modifies the strong disorder / low conductance behavior of the AII class [31, 32, 33], but plays not role in the weak disorder regime. Hence the behaviors of the first two cumulants in the weak localization regime of the single Dirac model with scalar disorder are exactly those of the standard AII / symplectic class. Moreover adding the HW term H_w does not break Time Reversal Symmetry, and thus does not change the universal symmetry class. In contrast, either a magnetic disorder or a magnetic field introduced through a Zeeman or orbital term in the Hamiltonian breaks time-reversal symmetry and induces a crossover from the AII/symplectic to the A/unitary class characterized by the absence of time reversal symmetry. Such a crossover between the symplectic and unitary ensembles has already been observed by depositing Fe impurities at the surface of ultrathin samples of Bi_2Te_3 [16]. In this experiment, the exchange field of the Fe atoms induces the Zeeman coupling for the SS carriers and destroys the weak antilocalization signature. Nevertheless the extreme thickness of the sample is likely to yield an important hybridization between the bulk, and top/bottom SSs while here we consider the response of a single isolated SS.

One of the characterizations of Anderson universality symmetry classes is the number of independent low energy modes in the diffusive regime. Those modes correspond to the various Cooperon/Diffuson modes which indeed parametrize the target space of the underlying non-linear sigma field theory. The symplectic class corresponds to two modes, one singlet Diffuson mode and one singlet Cooperon mode [36]. The breaking of time reversal symmetry by *e.g.* an orbital magnetic field will suppress the Cooperons whose propagator acquires a mass and is no longer diffusive : this induces a cross-over from the symplectic class to the unitary class, characterized by a single diffusive mode. This cross-over occurs on a length-scale determined by the mass acquired by the Cooperon singlet. The suppression of the Cooperon is attributed to destructive interference between time-reversed paths, accounted for by the retarded and advanced Green's functions in the Kubo formula. Such a cross-over will be discussed in section 5.4.

5.2. Weak antilocalization

When winding around the Fermi surface, the spinorial electron wave function acquires a π Berry phase which is responsible for weak antilocalization (WAL) phenomenon. In graphene, the presence of intervalley scattering leads to a crossover from weak antilocalization to weak localization when the ratio of intervalley over intravalley scattering rates is increased [35, 39]. In contrast, TIs with a single Dirac cone provide

ideal systems to measure WAL once the issue of the spurious bulk conductance is solved. Actually some experiments have already reported a strong WAL signal in thin films and in 3D HgTe slabs [15].

The quantum correction to the conductivity in the class AII corresponds to a weak anti localization correction : its determination within diagrammatic theory for Dirac fermions is recalled in Appendix B. In the limit of a phase coherent sample of size $L_\phi \ll L$ where L_ϕ is the phase coherent length, it reads:

$$\langle \delta\sigma \rangle = \left(\frac{e^2}{\pi\hbar}\right) \int_{\vec{Q}} \frac{1}{Q^2} = \frac{e^2}{\pi h} \ln(L_\phi/\ell_e) \tag{31}$$

where ℓ_e is the elastic mean free path. This result is independent of the particular model within the class AII. However, it depends on the the amplitude b of warping at high Fermi energy through the diffusion coefficient entering the phase coherence length $L_\phi = \sqrt{D(b)\tau_\phi}$, where τ_ϕ is the phase coherence time.

When a transverse magnetic field is applied, the standard derivation to account for the magnetic orbital effect of this result still holds [36]: it amounts to derive the Cooperon contribution from the probability of return to the origin of a diffusive path in the presence of the magnetic field. The corresponding correction to the conductivity is thus given by [36]:

$$\langle \delta\sigma(B) \rangle = \frac{e^2}{4\pi^2\hbar} \left[\Psi\left(\frac{1}{2} + \frac{B_e}{B}\right) - \Psi\left(\frac{1}{2} + \frac{B_\phi}{B}\right) \right], \tag{32}$$

where the characteristic fields $B_e = \hbar/(4eD(b)\tau_e)$ and $B_\phi = \hbar/(4eD(b)\tau_\phi)$ have been introduced, and where Ψ is the Digamma function. The diffusion constant $D(b)$, non perturbative in b, is given by Eq.(30). This corresponds to the result obtained for graphene when inter-valley scattering can be neglected [35]. In our case, this expression implies that in a given sample, the shape of the weak anti-localization correction as a function of B will evolve as the Fermi energy is varied within the Topological Insulator gap and the warping amplitude b is varied. This effect will be discussed further in section 6.

5.3. Universal Conductance Fluctuations

As explained above, in the absence of magnetic field the Universal Conductance Fluctuations (UCF) result for the symplectic class results still holds and one finds, similarly to graphene [40] :

$$\langle \delta\sigma^2 \rangle = 12 \left(\frac{e^2}{h}\right)^2 \frac{1}{V} \int_{\vec{q}} \frac{1}{q^4}. \tag{33}$$

The derivation of this result for Dirac fermions is recalled in Appendix C. Defining the phase coherent $L_\phi = \sqrt{D(b)\tau_\phi(T)}$ and thermal lengthscales $L_T = \sqrt{\hbar D(b)/T}$, we can focus on different regimes : for $L \ll L_\phi, L_T$, a proper regularization of the integral in (33) leads to the universal value

$$\langle \delta\sigma^2 \rangle = \frac{12}{\pi^4} \left(\frac{e^2}{h}\right)^2 \sum_{n_x=1}^{\infty} \sum_{n_y=0}^{\infty} \frac{1}{(n_x^2 + n_y^2)^2} \simeq 0.185613 \left(\frac{e^2}{h}\right)^2. \tag{34}$$

This result is independent of the diffusion coefficient $D(b)$ and thus independent of the warping amplitude. On the other hand, in the other limits [36]:

$$\langle \delta\sigma^2 \rangle \simeq \frac{3}{\pi} \left(\frac{e^2}{h}\right)^2 \left(\frac{L_\phi}{L}\right)^2 \text{ for } L_\phi \ll L, L_T, \tag{35}$$

$$\simeq \left(\frac{L_T}{L}\right)^2 \left(\frac{e^2}{h}\right)^2 \ln\left(\frac{L}{L_T}\right) \text{ for } L_T \ll L \ll L_\phi, \tag{36}$$

$$\simeq \left(\frac{L_T}{L}\right)^2 \left(\frac{e^2}{h}\right)^2 \ln\left(\frac{L_\phi}{L_T}\right) \text{ for } L_T \ll L_\phi \ll L. \tag{37}$$

Hence a strong dependence of these UCF on the Fermi energy through the warping amplitude b is found in all these cases. The introduction of a transverse magnetic field induces a crossover from the symplectic class to the unitary class, where the amplitude of the fluctuations is reduced by a factor of two. This crossover is described as [36] :

$$\langle \delta\sigma(B)^2 \rangle = \frac{1}{2} \langle \delta\sigma^2 \rangle \left[1 + \frac{B_\phi}{B} \Psi'(\frac{1}{2} + \frac{B_\phi}{B})\right] \tag{38}$$

where Ψ is the Digamma function and $B_\phi(b) = \hbar/4eD(b)\tau_\phi$. The dependence in b of the diffusion constant will affect the value of B_ϕ : this characteristic field for the suppression of the WAL correction and this reduction by a factor 2 of the conductance fluctuations will decrease when the Fermi level is raised away from the Dirac point.

5.4. In-plane magnetic field: interplay between Zeeman and warping effects

We now consider the effect of an in plane Zeeman field on the transport properties of these Dirac fermions. This can be accounted for by adding to the Hamiltonian (1) a term

$$H_Z = g\mu_B \left(\sigma_x B_x + \sigma_y B_y\right). \tag{39}$$

Without warping, such a Zeeman field acts exactly like a constant vector potential and can be gauged away. This amounts to shift uniformly the momenta by $-g\mu_B \vec{B}/(\hbar v_F)$. Hence without warping, an in-plane Zeeman field does not modify the scattering properties of an (infinite) disordered sample. However the presence of the hexagonal warping term in (1) breaks this invariance : the shape of the Fermi surface is now modified by the Zeeman field. As a consequence, the scattering amplitudes $f(\theta, \theta' - \theta)$ acquire also a $\vec{B}$ dependence. We can naturally expect that this Zeeman field which modifies the scattering amplitudes redistributes the scattering matrix of the samples, and leads to conductance fluctuations induced by an in-plane magnetic field.

To describe quantitatively the effect of this Zeeman field, we extend the above diagrammatic analysis perturbatively in $\tilde{B} = g\mu_B B/E_F$. This Zeeman field, which breaks time reversal symmetry, induces a crossover from the symplectic to the unitary class. This crossover can be accounted for by the evolution of the Cooperon structure factor : its singular part does not correspond anymore to a diffusive singlet component but to the diffusion of a massive singlet:

$$\Gamma^C(\vec{Q}) = \frac{\gamma}{Dq^2\tau_e + m(b, \tilde{B})} |S\rangle\langle S|. \tag{40}$$

The mass $m(b,\tilde{B})$ which encodes the effects of the Zeeman field, is calculated perturbatively to the second order in $\tilde{B}$: $m(b,\tilde{B}) = m(b)\tilde{B}^2$. The non-perturbative result is represented in Fig. 8. We recover the expected result $m(0,\tilde{B}) = m(b,0) = 0$ corresponding to the single singlet diffusive Cooperon mode of the symplectic class. This

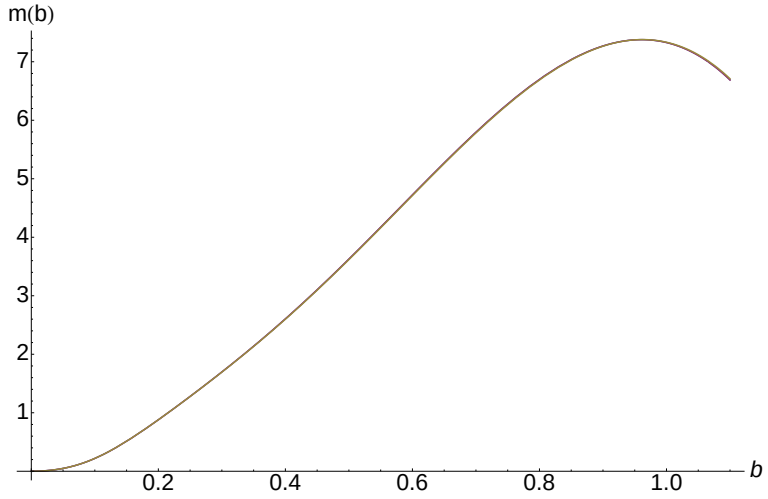

Figure 8. Evolution of the massive term $m(b)$ in the diffusion equation of the Cooperon, in presence of the hexagonal warping and in-plane Zeeman magnetic field, as a function of the warping parameter b.

mass is associated with a length parameterizing the cross-over from the symplectic to the unitary class, defined by $L_B = \sqrt{D\tau_e/m(b,B)}$. Beyond this length scale, we recover a standard unitary weak localization, and conductance fluctuations are reduced by a factor 2 :

$$\langle \delta\sigma(\vec{B})\rangle = \left(\frac{e^2}{\pi\hbar}\right)\int_{\vec{Q}} \frac{1}{Q^2 + L_B^{-2} + L_\phi^{-2}} = f(\tilde{L}/\ell_e, L/\tilde{L}) \tag{41}$$

$$\begin{aligned}\langle \delta\sigma^2(\vec{B})\rangle &= 6\left(\frac{e^2}{h}\right)^2 \frac{1}{V}\left[\int_{\vec{q}} \frac{1}{(q^2+L_\phi^{-2})^2} + \int_{\vec{q}} \frac{1}{(q^2+L_B^{-2}+L_\phi^{-2})^2}\right] \\ &= \frac{1}{2}\langle \delta\sigma^2(\vec{B}=\vec{0})\rangle + f_2(L/\tilde{L}),\end{aligned} \tag{42}$$

where L is the longitudinal size of the topological insulator surface, L_ϕ is the phase coherence length and $\tilde{L}$ is defined as $\tilde{L}^{-2} = L_B^{-2} + L_\phi^{-2}$. The function f and f_2 depends on the geometry of the sample. In the case of an infinite 2D sample, one recovers only a logarithmic dependence on $\tilde{L}/\ell_e$ for f. For a finite size sample, one has to to replace the integral by a sum over the compatible wavevectors[36].

As expected, we find that the UCF extrapolates between the value for the symplectic and the unitary class, over the length scale $L_B(b,B)$. An estimation of the evaluation of this length as a function of the magnetic field or the warping term is given by :

$$\frac{L_B}{\ell_e} = \frac{\sqrt{D(b)/D(b=0)m(b)}}{\tilde{B}} = \frac{c(b)}{\tilde{B}}, \tag{43}$$

where the evolution $c(b)$ with the warping amplitude is shown in Fig. 9 For experimental realistic values, $b \simeq 0.7$, $c(0.7) \simeq 1$, $E_F \simeq 0.3 \quad eV$ and $g\mu_B \simeq 5.10^{-4} \quad eV.T^{-1}$. This gives for a magnetic field around 1 T a characteristic length to observe the crossover $L_B \simeq 1000\ \ell_e$ which is is rather large but within experimental reach.

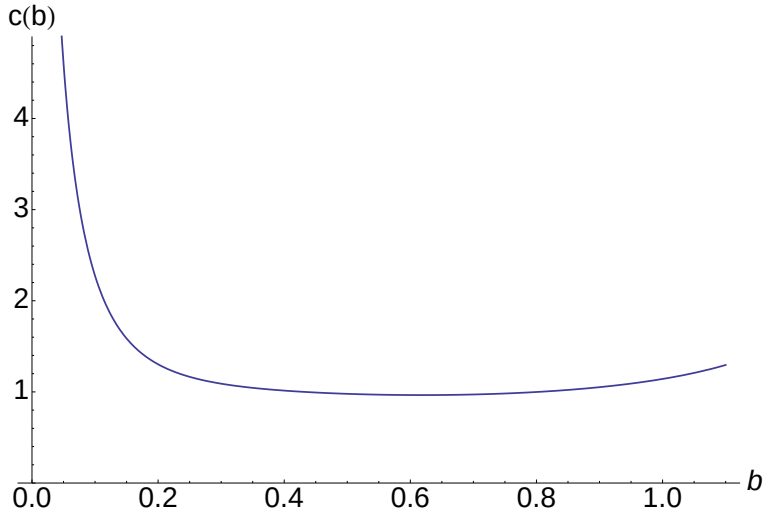

Figure 9. Dependence in b of the characteristic length to observe the crossover from symplectic to unitary class, for an in-plane Zeeman magnetic field.

6. Summary of Results and Conclusions

In this section, we summarize the main results of our approach focusing on the experimentally relevant aspects. In particular, we emphasize the effect of strong variation of the warping amplitude b as the Fermi energy is varied in a given material. Universal properties of transport in the quantum regime are not affected by the presence of this warping. However, both the departure from these universal properties as well as the classical regime are entirely characterized by the diffusion constant $D(b)$ which itself depends in the warping amplitude.

The transport properties in the incoherent classical regime are characterized by both the density of states $\rho(E_F)$ and the diffusion constant D. The dependence on the Fermi energy of both quantities is strongly affected by the presence of the warping of the Fermi surface, whose amplitude b itself depends on E_F. This is shown on Fig. 10,11 for two sets of parameters corresponding to the Bi_2Se_3 and Bi_2Te_3 compounds. As a consequence of these results, the conductivity σ acquires a strong Fermi energy dependence shown on Fig. 11, which can be directly probed experimentally.

Similarly, the quantum corrections to transport depends strongly on the Fermi energy through the dependence of the Diffusion coefficient D on the warping amplitude. Indeed, the shape of the typical measurement of the weak (anti-)localization correction through the dependence of the conductivity on a magnetic field perpendicular to the surface depends solely on the diffusion constant. This diffusion constant depending on

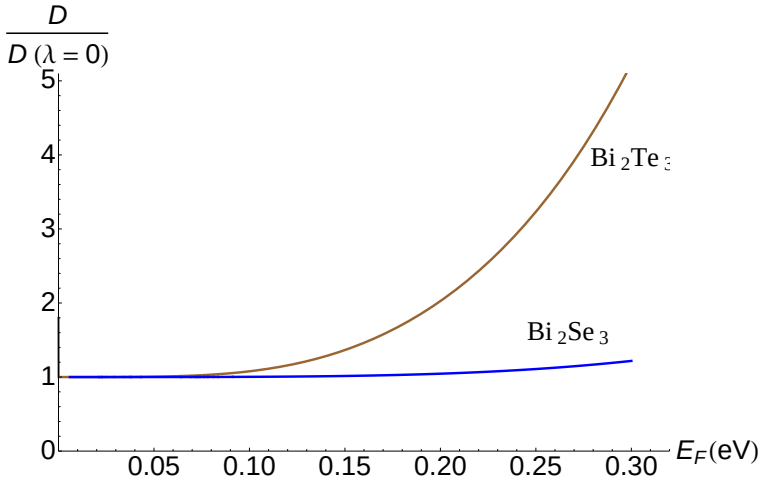

Figure 10. Dependence of the diffusion constant on the Fermi energy for the values of λ, v_F corresponding to the Bi_2Se_3 and Bi_2Te_3 compounds. The results depend on the amplitude of disorder parameterized by the mean free path l_e. Here, they are normalized with respect to the diffusion constant in absence of warping $D(\lambda = 0)$ which is independent of the Fermi energy and incorporates the dependence on l_e.

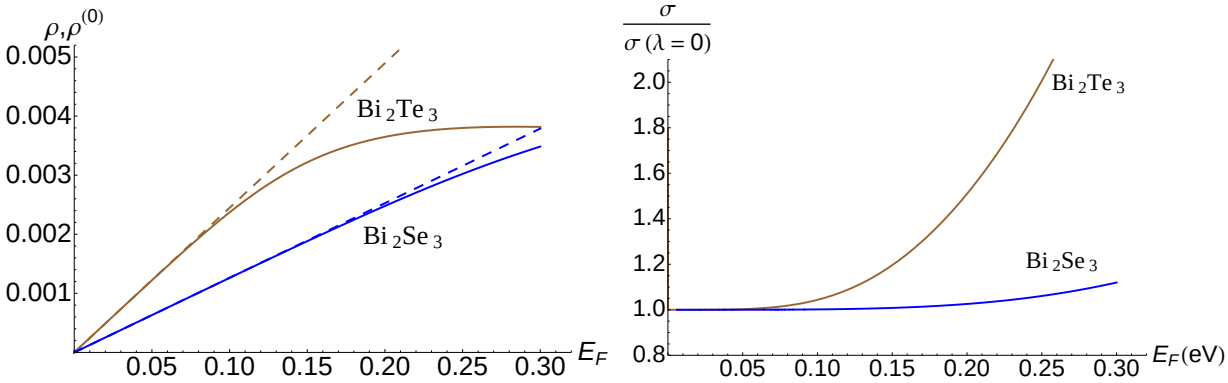

Figure 11. Dependence of the density of states (Left) and classical conductivity (Right) on the Fermi energy for values of $\lambda = 128$ eV.$\mathring{A}^3$, $v_F = 3.55$ eV.$\mathring{A}$ for Bi_2Se_3 and $\lambda = 250$ eV.$\mathring{A}^3$ and $v_F = 2.55$ eV.$\mathring{A}$ corresponding to the Bi_2Te_3 compounds. On the left figure, the dotted lines corresponds to the standard linear density of states for Dirac fermions without warping $\lambda = 0$. On the right figure, the results are represented as a ratio with the conductivity in the absence of warping $\sigma(\lambda = 0)$ which is independent on the energy and incorporates the dependence on the disorder strength.

the Fermi energy, the associated anti-localization curve depends itself on this Fermi energy as shown on Fig. 12. While the amplitude of conductance fluctuations are universal in the limit of an entirely coherent conductor, their amplitude in a realistic situation where $L_\phi \simeq L$ will be parameterized by a universal function of the diffusion coefficient. We have shown moreover that these fluctuations depend in a remarkable way on an in-plane Zeeman magnetic field. The amplitude of this effect depends on the ratio between the associated magnetic dephasing length L_B and the mean free path ℓ_e.

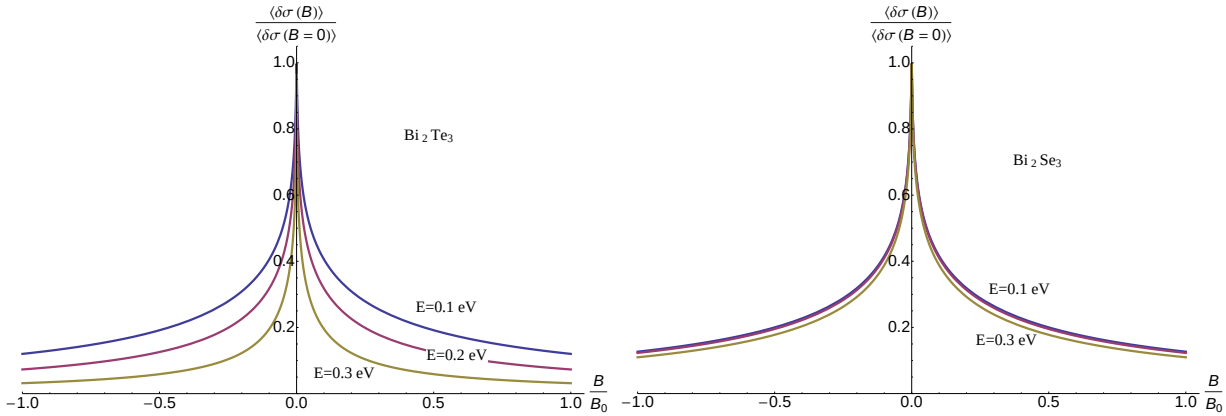

Figure 12. Dependence of the weak localization correction $\langle\delta\sigma(B)\rangle/\langle\delta\sigma(B=0)\rangle$ on the Fermi energy for the values of λ, v_F corresponding to the Bi_2Te_3 (Left) and Bi_2Se_3 (Right) compounds. We have chosen to scale the magnetic field as B/B_0 where $B_0 l_e^2 = \phi_0 = h/e$ to avoid any energy (or warping) dependence of this rescaling field. The results show a clear dependence on energy of the magnetic field characteristic of weak localization decay.

The dependence of this ratio on the Fermi energy is shown on Fig. 13 for the two same sets of values used above.

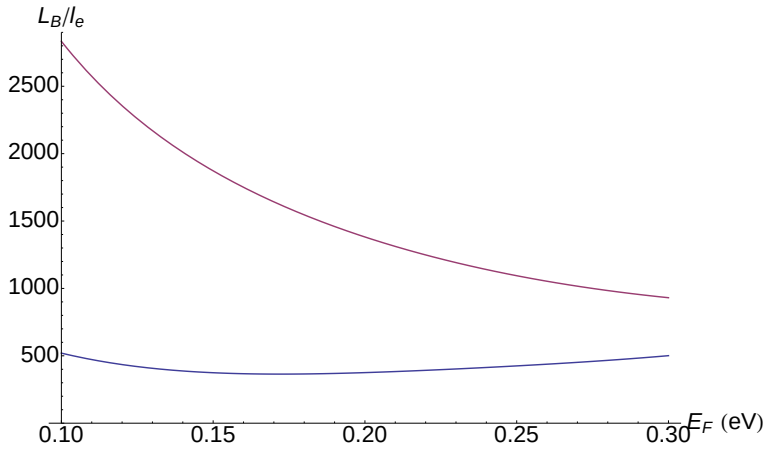

Figure 13. Dependence of the magnetic dephasing length L_B on the Fermi energy for parameters corresponding to Bi_2Te_3 (Red) and Bi_2Se_3 compounds.

In conclusion, we have shown that it is essential to take into account the hexagonal deformation of the Dirac cone occurring at the surface of topological insulators such as Bi_2Se_3 and Bi_2Te_3 to accurately describe both their classical and quantum transport properties. In particular, we provide a formula describing the evolution of diffusion constant D for arbitrary strength of the warping. Since this warping amplitude increases with the Fermi energy of the surface states, we predict a dependance on doping of transport properties different from those predicted for a perfect Dirac cone.

This work was supported by the ANR under the project 2010-BLANC-041902 (ISOTOP). JC also acknowledges support from EU/FP7 under contract TEMSSOC.

Appendix A. Non Perturbative Density of states

In the presence of warping, the density of states at the Fermi level $\rho(\epsilon_F)$ is modified. One has:

$$\rho(\epsilon) = \int_0^{+\infty} \frac{kdk}{2\pi} \int_0^{2\pi} \frac{d\theta}{2\pi} \delta\left[\epsilon - \sqrt{(\hbar v k)^2 + \lambda^2 k^6 \cos^2(3\theta)}\right]. \tag{A.1}$$

Performing the angular integration first, the density of states is obtained as the integral:

$$\rho(\epsilon) = \frac{\epsilon}{2(\pi\hbar v)^2} \int_{y_-}^1 \frac{dy}{\sqrt{(1-y)(4b^2y^3+y-1)}}, \tag{A.2}$$

where y_- is the unique real solution of the equation $4b^2y^3 + y - 1 = 0$. By the usual formula for solving equations of the third degree, we have:

$$y_- = \frac{1}{2\sqrt{3}b}\left[\sqrt[3]{3\sqrt{3}b + \sqrt{1+27b^2}} - \sqrt[3]{\sqrt{1+27b^2} - 3\sqrt{3}b}\right]. \tag{A.3}$$

It is convenient to introduce the parameterization $\sinh\varphi = 3\sqrt{3}b$, giving $y_- = 3\sinh(\varphi/3)/\sinh\varphi$. With the change of variables $y_- = 1 - 1/t$, the integral in (A.2) can be rewritten:

$$\rho(\epsilon) = \frac{\epsilon}{2\sqrt{2}b(\pi\hbar v)^2} \int_{t_-}^{+\infty} \frac{dt}{\sqrt{(t-1)^3 - t^2/(2b^2)}}. \tag{A.4}$$

Using Eqs. (17.4.70)–(17.4.72) from [41], the integral in Eq. (A.4) can be expressed in terms of a complete elliptic integral of the first kind, giving the density of states:

$$\rho(\epsilon) = \frac{\epsilon}{2(\pi\hbar v)^2} \frac{2K\left[\frac{1}{2} - \frac{1}{4}\left(3 - \frac{1}{\left(1+\frac{4}{3}\sinh^2(\varphi/3)\right)^2}\right)\sqrt{\frac{1+\frac{4}{3}\sinh^2(\varphi/3)}{1+4\sinh^2(\varphi/3)}}\right]}{\left(1+\frac{4}{3}\sinh^2(\varphi/3)\right)^{3/4}\left(1+4\sinh^2(\varphi/3)\right)^{1/4}} \tag{A.5}$$

In the limit of $\lambda \to 0$, $\varphi \to 0$, and (A.5) reduces to the density of states in the absence of warping. For large λ, we have $b \sim 2e^{\varphi}3\sqrt{3}$, and the density of states behaves as: $\rho(\epsilon) \sim 3^{-1/4}\pi^{-2}K(1/2 - \sqrt{3}/4)(\epsilon\lambda^2)^{-1/3}$. Since the density of states goes to zero for large and small energy, it has a maximum at a finite value of ϵ. By simple scaling, the maximum is obtained for an energy $\epsilon^* = C_1\sqrt{(\hbar v_F)^3/\lambda}$ and $\rho(\epsilon^*) = C_2(\hbar v_F\lambda)^{-1/2}$.

Appendix B. Weak anti-localization correction for Dirac fermions

In this appendix, we derive the quantum correction to conductivity for two dimensional Dirac fermions in the absence of warping ($b = 0$). In this case of linearly dispersing Dirac fermions, the current operator $j_x = -ev_F\sigma^x$ is no longer a function of $\vec{k}$. The renormalization of this current operator by vertex corrections can be written as

$$\Sigma^x = j_x + j_x P^D \Gamma^D = 2j_x \tag{B.1}$$

where Σ^x stands for the renormalized operator. The quantum corrections to conductivity are associated with contributions between interferences of loops of diffusive paths. This interference between a loop and its time-reversed contribution is described as the

propagation of the so-called *Cooperon*. Its propagator is defined through the Dyson equation $\Gamma^C(\vec{Q},\omega) = \gamma[\mathbb{1}\otimes\mathbb{1} - \gamma P^C(\vec{Q},\omega)]$ where P^C is :

$$P^{(C)}(\vec{Q},\omega) = \int \frac{d\vec{k}}{(2\pi)^2} \langle G^R(\vec{k},E)\rangle \ \langle G^A(\vec{Q}-\vec{k},E-\omega)\rangle. \tag{B.2}$$

By a time-reversal operation on the advanced component, we can relate the Cooperon to the previously identified Diffuson propagator. Only the diffusive modes of the Cooperon contribute to the dominant quantum correction, leading to a structure factor for the Cooperon :

$$\Gamma^C(\vec{Q}) = \frac{\gamma}{\tau_e}\frac{1}{DQ^2}|S\rangle\langle S| \tag{B.3}$$

$$= \frac{\gamma}{\tau_e}\frac{1}{DQ^2}\frac{1}{4}\left[\mathbb{1}\otimes\mathbb{1} - \sigma^x\otimes\sigma^x - \sigma^y\otimes\sigma^y - \sigma^z\otimes\sigma^z\right], \tag{B.4}$$

where D is the diffusion constant, $D = v_F^2\tau_e$ in the absence of warping.

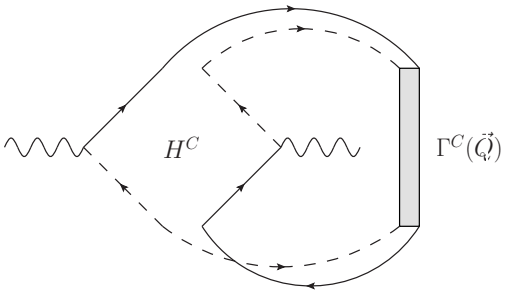

Figure B1. Diagrammatic representation of the quantum correction to conductivity

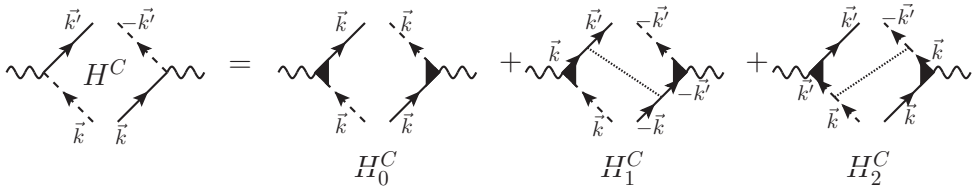

Figure B2. Diagrammatic representation of the dressing of the Hikami box

The weak anti-localization correction is obtained by the contraction of a Cooperon propagator and a Hikami box, as represented diagrammatically on Fig. B1. This Hikami box is the sum of three different contributions represented in Fig. B2. We express the first of these contributions as

$$\langle\delta\sigma_0\rangle = \frac{\hbar}{2\pi}\mathrm{Tr}\left[G^A(\vec{k})\Sigma^x G^R(\vec{k})\Gamma^C(\vec{Q})G^R(\vec{Q}-\vec{k})\Sigma^x G^A(\vec{Q}-\vec{k})\right], \tag{B.5}$$

where we used the notations introduced in the article Tr for the trace over all the quantum numbers (spin and momenta), tr for the trace over the spin indices, and $\int_{\vec{k}}$ for the trace over the momentum $\vec{k}$. Special care has to be devoted to the order

of the spin indices in these expressions. In the expression Eq.(B.5), the $\vec{Q}$ integral is dominated by the small $\vec{Q}$ contribution originating from the diffusive modes of the Cooperon. This justifies *a posteriori* the projection on the single diffusive mode in (B.3). Focusing on the most dominant part of this expression, we can set $Q \to 0$ except in the Cooperon propagator, the Green's functions being regular in $\vec{k}$. Similarly, we can pull the renormalized vertices out of the integral and focus on the Hikami box :

$$\begin{aligned} H_0^C &= 4 \int_{\vec{k}} \left[G^A(\vec{k}) \sigma^x G^R(\vec{k}) \right] \otimes \left[G^R(-\vec{k}) \sigma^x G^A(-\vec{k}) \right] \\ &= \rho(E_F) \left(\frac{2\tau_e}{\hbar} \right)^3 \frac{\pi}{16} \left[3\sigma^x \otimes \sigma^x + \sigma^y \otimes \sigma^y - 4\, \mathbb{1} \otimes \mathbb{1} \right]. \end{aligned} \tag{B.6}$$

Similarly, the two remaining diagrams contributing to the Hikami box in Fig. B2 are expressed as

$$\begin{aligned} H_1^C &= 4\gamma \int_{\vec{k}} \int_{\vec{q}_1} \left[G^A(\vec{k}) \sigma^x G^R(\vec{k}) G^R(-\vec{q}_1) \right] \otimes \left[G^R(-\vec{k}) G^R(\vec{q}_1) \sigma^x G^A(\vec{q}_1) \right] \\ &= \frac{\pi}{16} \rho(E_F) \left(\frac{2\tau_e}{\hbar} \right)^3 \left[\mathbb{1} \otimes \mathbb{1} - \sigma^x \otimes \sigma^x \right] \end{aligned} \tag{B.7}$$

and :

$$\begin{aligned} H_2^C &= 4\gamma \int_{\vec{k}} \int_{\vec{q}_1} \left[G^A(-\vec{q}_1) G^A(\vec{k}) \sigma^x G^R(\vec{k}) \right] \otimes \left[G^R(\vec{q}_1) \sigma^x G^A(\vec{q}_1) G^A(-\vec{k}) \right] \\ &= \frac{\pi}{16} \rho(E_F) \left(\frac{2\tau_e}{\hbar} \right)^3 \left[\mathbb{1} \otimes \mathbb{1} - \sigma^x \otimes \sigma^x \right] \end{aligned} \tag{B.8}$$

Summing these three contributions we obtain :

$$H^C = \rho(E_F) \left(\frac{2\tau_e}{\hbar} \right)^3 \frac{\pi}{16} \left[\sigma^x \otimes \sigma^x + \sigma^y \otimes \sigma^y - 2\, \mathbb{1} \otimes \mathbb{1} \right]. \tag{B.9}$$

The resulting weak anti localization correction is obtained *via* the final contraction with a Cooperon propagator as shown on Fig.B1, and leads to the expression:

$$\begin{aligned} \langle \delta\sigma \rangle &= \frac{\hbar \rho(E_F) (-e v_F)^2}{2\pi} \left(\frac{2\tau_e}{\hbar} \right)^3 \frac{\pi}{16} \mathrm{tr} \left(\sigma^x \otimes \sigma^x + \sigma^y \otimes \sigma^y - 2\, \mathbb{1} \otimes \mathbb{1} \right) \int_{\vec{Q}} \Gamma(\vec{Q}) \\ &= \left(\frac{e^2}{\pi\hbar} \right) \int_{\vec{Q}} \frac{1}{Q^2} \end{aligned} \tag{B.10}$$

Appendix C. Universal Conductance Fluctuations for Dirac fermions

To derive the conductance fluctuations, we need to take into account two kinds of diagrams containing either Cooperons or Diffusons. The Hikami box for Cooperons has been calculated previously. Proceeding similarly with the Diffuson instead of Cooperon structure factor we obtain the Hikami box for Diffusons :

$$H^D = \rho(E_F) \left(\frac{2\tau_e}{\hbar} \right)^3 \frac{\pi}{16} \left[2\, \mathbb{1} \otimes \mathbb{1} + \sigma^x \otimes \sigma^x + \sigma^y \otimes \sigma^y \right]. \tag{C.1}$$

We have already performed an integration over the momentum (arising from the Kubo formula) in these expressions for the Hikami boxes. Hence we only need to plug a

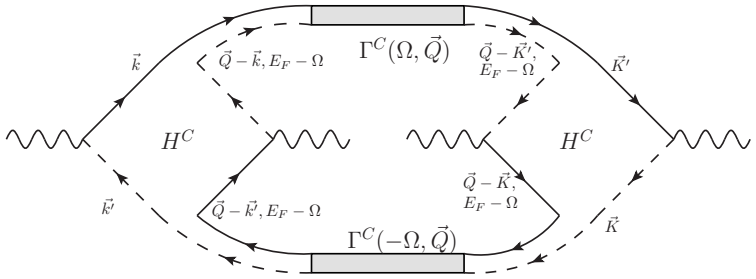

Figure C1. Diagram for the conductance fluctuations with Cooperons

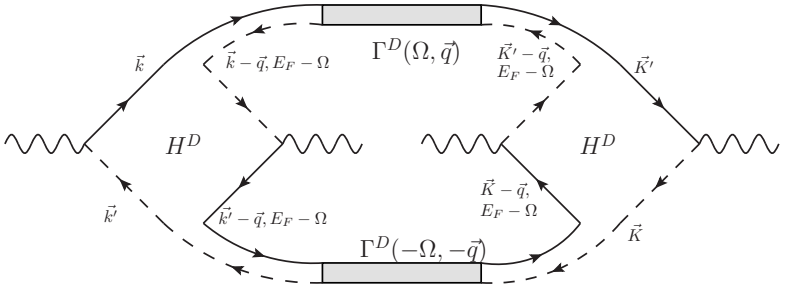

Figure C2. Diagram for the conductance fluctuations with Diffusons.

Diffuson (resp. Cooperon) structure factor between two H^D (resp. H^C). Summing these two diagrams (Fig. C2 and Fig. C1) we obtain :

$$\langle \delta\sigma_1^2 \rangle = 8 \left(\frac{e^2}{h}\right)^2 \frac{1}{V}\int_{\vec{q}} \frac{1}{q^4}. \tag{C.2}$$

The second part of the conductance fluctuations come from the diagrams represented in Fig. C3 that we have not yet considered. They require the determination of two additional Hikami boxes (one for Diffusons and one for Cooperons) :

$$\tilde{H}^D = \rho(E_F) \left(\frac{2\tau_e}{\hbar}\right)^3 \frac{\pi}{16} \left[\mathbb{1}\otimes\mathbb{1} + \sigma^x \otimes \sigma^x\right] \tag{C.3}$$

$$\tilde{H}^C = \rho(E_F) \left(\frac{2\tau_e}{\hbar}\right)^3 \frac{\pi}{16} \left[\mathbb{1}\otimes\mathbb{1} - \sigma^x \otimes \sigma^x\right]. \tag{C.4}$$

The final results after contraction in spin space of these diagrams is

$$\langle \delta\sigma_2^2 \rangle = 4 \left(\frac{e^2}{h}\right)^2 \frac{1}{V}\int_{\vec{q}} \frac{1}{q^4}. \tag{C.5}$$

Summing the two contributions (C.2) and (C.5), we finally get the result of Eq 33 :

$$\langle \delta\sigma^2 \rangle = \langle \delta\sigma_1^2 \rangle + \langle \delta\sigma_2^2 \rangle = 12 \left(\frac{e^2}{h}\right)^2 \frac{1}{V}\int_{\vec{q}} \frac{1}{q^4} \tag{C.6}$$

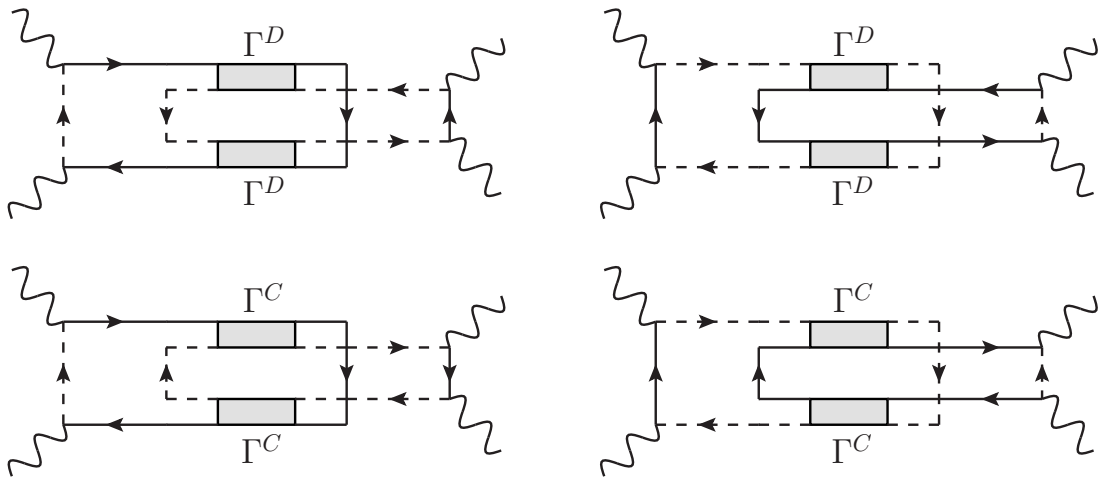

Figure C3. Diagrams for the second contribution to conductance fluctuations

Appendix D. Quantum correction for a warped Fermi surface

Appendix B and Appendix C show explicitly the derivation of the weak antilocalization correction and the conductance fluctuations for Dirac fermions. As expected, the corresponding results display no dependence in the only relevant parameter to characterize diffusion : the diffusion constant. These results are naturally expected to hold when taking into account the hexagonal warping term. To explicitly show this independence, we determine the value of the quantum correction to conductivity in the general case where the Fermi surface possesses the hexagonal deformation.

The first step is to obtain the new Hikami box H^C, the difficulty arising from the dependence of the current operator on the momentum $j_x = e\left(-v_F\sigma_x + \frac{3\lambda}{\hbar}\sigma_z(k_x^2 - k_y^2)\right)$. Recalling that $\Sigma^x = j_x + j_x P^D \Gamma^D$, we express the "naked" Hikami box as:

$$H_0^C = \int_{\vec{k}} \left[G^A(\vec{k})\Sigma^x G^R(\vec{k}) G^R(-\vec{k})\Sigma^x G^A(-\vec{k}) \right]. \tag{D.1}$$

We perform this integral using polar coordinates, and integrate the radial part :

$$H_0^C = \frac{e^2 v_F^2 \tau_e^2}{4\gamma\hbar} \frac{\tau_e}{\tau_e^{(0)}} \int \frac{d\theta}{2\pi} \frac{A_+ B A_+ \otimes A_- B A_-}{1 + 12 b^2 \tilde{k}(\theta)^4 \cos^2(3\theta)} \tag{D.2}$$

$$A_\pm = \mathbb{1} \pm \tilde{k}(\theta)\left(\cos\theta\sigma^x + \sin\theta\sigma^y\right) + 2b\ \tilde{k}^3(\theta)\cos(3\theta)\sigma^z \tag{D.3}$$

$$B = \left(2 + \frac{\beta}{\alpha+\beta}\right)\sigma^x + 6b\ \tilde{k}^2(\theta)\cos(2\theta)\sigma^z \tag{D.4}$$

The two "dressed" Hikami boxes, where an impurity line links two Green's functions can be calculated by the method used above, and we can write the result as $H^C = \frac{e^2 v_F^2 \tau_e^2}{4\gamma\hbar} H(b)$. We need to close this Hikami box with a Cooperon structure factor $\Gamma^C = \frac{\gamma}{\tau_e}\frac{1}{D(b)Q^2}\frac{1}{4}\left(\mathbb{1}\otimes\mathbb{1} - \sigma^x\otimes\sigma^x - \sigma^y\otimes\sigma^y - \sigma^z\otimes\sigma^z\right)$. Performing the sum on the spin space $h(b) = \mathrm{tr}[H(b)\frac{1}{4}\left(\mathbb{1}\otimes\mathbb{1} - \sigma^x\otimes\sigma^x - \sigma^y\otimes\sigma^y - \sigma^z\otimes\sigma^z\right)]$ we obtain the

quantum correction to the conductivity :

$$\langle \delta\sigma(b) \rangle = \frac{\hbar}{2\pi} \mathrm{Tr}(H^C \Gamma^C) = \frac{e^2}{h} \frac{v_F^2 \tau_e h(b)}{2D(b)} \int \frac{d\vec{q}}{q^2}. \tag{D.5}$$

We found numerically the correction $\frac{v_F^2 \tau_e h(b)}{2D(b)}$ to be constant equal to 1 and independent of b.

[1] M. Z. Hasan and C. L. Kane. Colloquium: Topological insulators. *Rev. Mod. Phys.*, 82:3045, 2010.

[2] Xiao-Liang Qi and Shou-Cheng Zhang. Topological insulators and superconductors. *Rev. Mod. Phys.*, 83:1057, 2011.

[3] Haijun Zhang, Chao-Xing Liu, Xiao-Liang Qi, Xi Dai, Zhong Fang, and Shou-Cheng Zhang. Topological insulators in Bi_2Se_3, Bi_2Te_3 and Sb_2Te_3 with a single dirac cone on the surface. *Nat. Phys.*, 5:438, 2009.

[4] Y. Xia, D. Qian, D. Hsieh, L. Wray, A. Pal, H. Lin, A. Bansil, D. Grauer, Y. S. Hor, R. J. Cava, and M. Z. Hasan. Observation of a large-gap topological-insulator class with a single dirac cone on the surface. *Nat. Phys.*, 5:398, 2009.

[5] Y. L. Chen, J. G. Analytis, J.-H. Chu, Z. K. Liu, S.-K. Mo, X. L. Qi, H. J. Zhang, D. H. Lu, X. Dai, Z. Fang, S. C. Zhang, I. R. Fisher, Z. Hussain, and Z.-X. Shen. Experimental realization of a three-dimensional topological insulator, Bi_2Te_3. *Science*, 325:178–181, 2009.

[6] D. Hsieh, Y. Xia, D. Qian, L. Wray, J. H. Dil, F. Meier, J. Osterwalder, L. Patthey, J. G. Checkelsky, N. P. Ong, A. V. Fedorov, H. Lin, A. Bansil, D. Grauer, Y. S. Hor, R. J. Cava, and M. Z. Hasan. A tunable topological insulator in the spin helical dirac transport regime. *Nature*, 460:1101, 2009.

[7] K. Eto, Z. Ren, A. Taskin, K. Segawa, and Y. Ando. Angular-dependent oscillations of the magnetoresistance in Bi_2Se_3 due to the three-dimensional bulk fermi surface. *Phys. Rev. B*, 81:195309, 2010.

[8] J. Analytis, J. Chu, Y. Chen, F. Corredor, R. McDonald, Z. Shen, and I. Fisher. Bulk fermi surface coexistence with dirac surface state in Bi_2Se_3: A comparison of photoemission and shubnikov–de haas measurements. *Phys. Rev. B*, 81:205407, 2010.

[9] N. Butch, K. Kirshenbaum, P. Syers, A. Sushkov, G. Jenkins, H. Drew, and J. Paglione. Strong surface scattering in ultrahigh-mobility Bi_2Se_3 topological insulator crystals. *Phys. Rev. B*, 81:241301(R), 2010.

[10] James G. Analytis, Ross D. McDonald, Scott C. Riggs, Jiun-Haw Chu, G. S. Boebinger, and Ian R. Fisher. Two-dimensional surface state in the quantum limit of a topological insulator. *Nat. Phys.*, 6:960, 2010.

[11] J. G. Checkelsky, Y. S. Hor, R. J. Cava, and N. P. Ong. Bulk band gap and surface state conduction observed in voltage-tuned crystals of the topological insulator Bi_2Se_3. *Phys. Rev. Lett.*, 106:196801, 2011.

[12] H. Steinberg, D. Gardner, Y. Lee, and P. Jarillo-Herrero. Surface state transport and ambipolar electric field effect in Bi_2Se_3 nanodevices. *Nano Lett.*, 10:5032, 2010.

[13] D. Kim, S. Cho, N.P. Butch, P. Syers, K. Kirshenbaum, J. Paglione, and M.S. Fuhrer. Minimum conductivity and charge inhomogeneity in Bi_2Se_3 in the topological regime. arXiv:1105.1410, 2011.

[14] D. Kong, W. Dang, J.J. Cha, H. Li, S. Meister, H. Peng, Z. Liu, and Y. Cui. Few-layer nanoplates of Bi_2Se_3 and Bi_2Te_3 with highly tunable chemical potential. *Nano Lett.*, 10:2245, 2010.

[15] C. Bouvier, T. Meunier, P. Ballet, X. Baudry, R. Kramer, and Laurent Levy. Strained HgTe: a textbook 3d topological insulator. arXiv:1112.2092, 2011.

[16] Hong-Tao He, Gan Wang, Tao Zhang, Iam-Keong Sou, George K. L Wong, Jian-Nong Wang, Hai-Zhou Lu, Shun-Qing Shen, and Fu-Chun Zhang. Impurity effect on weak antilocalization in the topological insulator Bi_2Te_3. *Phys. Rev. Lett.*, 106:166805, 2011.

[17] D. Culcer, E.H. Hwang, T.D. Stanescu, and S. Das Sarma. Two-dimensional surface charge transport in topological insulators. *Phys. Rev. B*, 82:155457, 2010.

[18] L. Fu. Hexagonal warping effects in the surface states of the topological insulator Bi_2Te_3. *Phys. Rev. Lett.*, 103:266801, 2009.

[19] Z. Alpichshev, J.G. Analytis, J.-H. Chu, I. R. Fisher, Y. L. Chen, Z. X. Shen, A. Fang, and A. Kapitulnik. STM imaging of electronic waves on the surface of Bi_2Te_3: Topologically protected surface states and hexagonal warping effects. *Phys. Rev. Lett.*, 104:016401, 2010.

[20] Z. Alpichshev, J. G. Analytis, J.-H. Chu, I. R. Fisher, and A. Kapitulnik. STM imaging of a bound state along a step on the surface of the topological insulator Bi_2Te_3. *Phys. Rev. B*, 84:041104, 2011.

[21] S. Souma, K. Kosaka, T. Sato, M. Komatsu, A. Takayama T. Takahashi, M. Kriener, Kouji Segawa, and Yoichi Ando. Direct measurement of the out-of-plane spin texture in the dirac-cone surface state of a topological insulator. *Phys. Rev. Lett.*, 106:216803, 2011.

[22] Su-Yang Xu, L. A. Wray, Y. Xia, F. von Rohr, Y. S. Hor, J. H. Dil, F. Meier, B. Slomski, J. Osterwalder, M. Neupane, H. Lin, A. Bansil, A. Fedorov, R. J. Cava, and M. Z. Hasan. Realization of an isolated dirac node and strongly modulated spin texture in the topological insulator Bi_2Te_3. arXiv:1101.3985, 2011.

[23] W. Jung, Yeongkwan Kim, Beomyoung Kim, Yoonyoung Koh, Chul Kim, Masaharu Matsunami, Shin ichi Kimura, Masashi Arita, Kenya Shimada, Jung Hoon Han, Juyoung Kim, Beongki Cho, and Changyoung Kim. Observation of warping effects in the band and angular momentum structures of topological insulator Bi_2Te_3. arXiv:1112.2476, 2011.

[24] K. Kuroda, M. Arita, K. Miyamoto, M. Ye, J. Jiang, A. Kimura, E. E. Krasovskii, E. V. Chulkov, H. Iwasawa, T. Okuda, K. Shimada, Y. Ueda, H. Namatame, and M. Taniguchi. Hexagonally Deformed Fermi Surface of the 3D Topological Insulator Bi_2Se_3. *Phys. Rev. Lett.*, 105:076802, 2010.

[25] T. Hirahara, Y. Sakamoto, Y. Takeichi, H. Miyazaki, S-I Kimura, I. Matsuda, A. Kakizaki, and S. Hasegawa. Anomalous transport in an n-type topological insulator ultrathin Bi_2Se_3 film. *Phys. Rev. B*, 82:155309, 2010.

[26] Oleg V. Yazyev, Joel E. Moore, and Steven G. Louie. Spin polarization and transport of surface states in the topological insulators Bi_2Se_3 and Bi_2Te_3 from first principles. *Phys. Rev. Lett.*, 105:266806, 2010.

[27] G. Tkachov and E. M. Hankiewicz. Weak antilocalization in HgTe quantum wells and topological surface states: Massive versus massless dirac fermions. *Phys. Rev. B*, 84:035444, 2011.

[28] C. M. Wang and F. J. Yu. Effects of hexagonal warping on surface transport in topological insulators. *Phys. Rev. B*, 84:155440, 2011.

[29] Andreas P. Schnyder, Shinsei Ryu, Akira Furusaki, and Andreas W. W. Ludwig. Classification of topological insulators and superconductors in three spatial dimensions. *Phys. Rev. B*, 78:195125, 2008.

[30] A. P. Schnyder, S. Ryu, A. Furusaki, and A. W. W. Ludwig. Classification of topological insulators and superconductors. *AIP Conf. Proc.*, 10:1134, 2009.

[31] J. H. Bardarson, J. Tworzydło, P. W. Brouwer, and C. W. J. Beenakker. One-parameter scaling at the dirac point in graphene. *Phys. Rev. Lett.*, 99:106801, 2007.

[32] Kentaro Nomura, Mikito Koshino, and Shinsei Ryu. Topological delocalization of two-dimensional massless dirac fermions. *Phys. Rev. Lett.*, 99:146806, 2007.

[33] P.M. Ostrovsky, I.V. Gornyi, and A.D. Mirlin. Interaction-induced criticality in z2 topological insulators. *Phys. Rev. Lett.*, 105:036803, 2010.

[34] Chao-Xing Liu, Xiao-Liang Qi, HaiJun Zhang, Xi Dai, Zhong Fang, and Shou-Cheng Zhang. Model hamiltonian for topological insulators. *Phys. Rev. B*, 82:045122, 2010.

[35] E. McCann, K. Kechedzhi, V.I. Fal'ko, H. Suzuura, T. Ando, and B.L. Altshuler. Weak-localization magnetoresistance and valley symmetry in graphene. *Phys. Rev. Lett.*, 97:146805, 2006.

[36] E. Akkermans and G. Montambaux. *Mesoscopic Physics of Electrons and Photons*. Cambridge

University Press, 2007.

[37] A. Altland and M.R. Zirnbauer. Nonstandard symmetry classes in mesoscopic normal-superconducting hybrid structures. *Phys. Rev. B*, 55:1142, 1997.

[38] F. Evers and A. D. Mirlin. Anderson transitions. *Rev. Mod. Phys.*, 80:1355, 2008.

[39] F.V. Tikhonenko, A.A. Kozikov, A.K. Savchenko, and R.V. Gorbachev. Transition between electron localization and antilocalization in graphene. *Phys. Rev. Lett.*, 103:226801, 2009.

[40] M.Yu. Kharitonov and K.B. Efetov. Universal conductance fluctuations in graphene. *Phys. Rev. B*, 78:033404, 2008.

[41] M. Abramowitz and I. Stegun. *Handbook of mathematical functions.* Dover, New York, 1972.